International Journal of Physics and Mathematical Sciences ISSN: 2277-2111 (Online)
An Online International Journal Available at http://www.cibtech.org/jpms.htm
2012 Vol. 2 (3) July-September pp. 29-37/ Gurung
Research Article

PHOTOEMISSION STUDY OF METALS AND SEMICONDUCTORS BY USING A SPATIALLY VARYING VECTOR POTENTIAL

***Shivraj Gurung**
Department of Physics, Pachhunga University College, Aizawl-796 001, Mizoram
**Author for Correspondence*

ABSTRACT
The kronig-penney potential is used to define the crystal potential from which the wave function for the surface state is derived. The wave function thus obtained is used for photoemission calculations in the case of transition metals like *W* and *Ni* and semiconductors like lead salt using a spatially dependent vector potential. PACS: 79.60-i, 61.80Ba, 78.68+m, 41.20Jb

Key Words: *Photoemission, Photocurrent, Vector Potential, Dielectric Function*

INTRODUCTION

Photoemission technique has widely been considered as a means for studying the surface electronic state of solids. Photoemission is basically concerned with the excitation of electrons. These photo-excited electrons lying either at the surface or deep within the bulk have to gain sufficient energy such that they are transported across the surface potential barrier. The incident photon energy is too weak to impart the necessary momentum to photoexcite the surface electrons. The spatial variation of the vector potential at the surface has been considered to be the main factor responsible for initiating the photo excitation at the surface. Bagchi and Kar (1978) developed a dielectric model to deduce vector potential using a simple 'local' dielectric function and applied the same to study photoemission from tungsten. This model had been used by Thapa et al. in explaining the surface photoemission in metals like aluminium (Das *et al.,* (1991); Zaithanzauva and Thapa (1996), palladium (Thapa, 1991)), copper and molybdenum (Pachuau *et al.,* (2002)) and semiconductors like silicon and gallium arsenide (Thapa *et al.,* 1994; Pachuau *et al.,* 1999).

In this report, we will use a dielectric model for the surface which unlike the model of Bagchi and Kar (1978) interpolates logarithmically between the bulk value and the vacuum value (Gurung *et al.,* 2006). On the basis of this, an appropriate vector potential will be deduced which will be used for calculating photocurrent. Photocurrent will be calculated from metals *W* and *Ni* and semiconductors *PbS* and *PbSe.*

Formalism

Using Fermi golden rule (Penn (1972)), photocurrent density formula can be written as

$$\frac{dj(E)}{d\Omega} = \frac{2\pi}{\hbar}\sum_{f,i}\left|\langle\psi_f\left|H'\right|\psi_i\rangle\right|^2\delta\left(E_f - E_i - \hbar\omega\right)f_o(E-\hbar\omega)\left[1-f_o(E)\right] \qquad \ldots\ldots\ldots (1)$$

Where ψ_i and ψ_f are the initial and final state wave functions and $H' = \left(\frac{e}{2mc}\right)(\boldsymbol{A}\cdot\boldsymbol{p} + \boldsymbol{p}.\boldsymbol{A})$, $\boldsymbol{A}$ being the vector potential of the photon field and $\boldsymbol{p}$ the one electron momentum operator. To evaluate the matrix element, we have to evaluate $\boldsymbol{A}$ and construct ψ_i and ψ_f.

Dielectric Model and Vector Potential

We consider the solid to occupy all space to the left of $z = 0$ plane with surface parallel to the x-y plane and assume the surface region to extend from $z = 0$ to $z = -d$ such that the surface is of thickness d. The model dielectric function (Figure 1) for the bulk ($z \le -d$), surface ($-d \le z \le 0$) and vacuum ($z \ge 0$) is given by,

Research Article

$$\varepsilon(\omega,z)=\begin{cases}\varepsilon_b(\omega) & ;\ z\le -d\\ 1+\dfrac{(\varepsilon_b-1)}{\log_e 2}\log_e\left(1-\frac{z}{d}\right) & ;\ -d\le z\le 0\\ 1 & ;\ z\ge 0\end{cases} \quad \ldots\ldots\ldots (2)$$

Where $\varepsilon_b(\omega)\cong\varepsilon_1(\omega)+i\varepsilon_2(\omega)$ is the dielectric function for the bulk region? For a $p-$polarized light, the magnetic field $B(z)=B(\boldsymbol{K},\omega,z)$ (where $\boldsymbol{K}=\dfrac{\omega}{c}Sin\,\theta_i$) is in the y-direction and it obeys the following equation (Landau and Lifsitz, 1984)

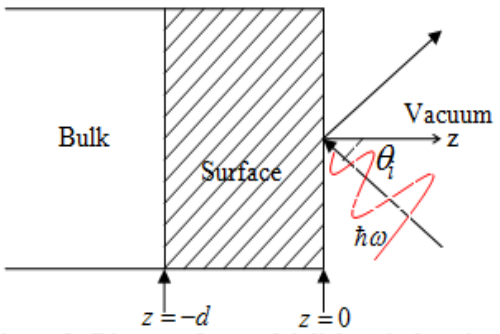

Figure 1: Diagram for model dielectric function

$$\frac{\partial}{\partial z}\left(\frac{1}{\varepsilon}\frac{\partial B}{\partial z}\right)+\left(\frac{\omega^2}{c^2}-\frac{K^2}{\varepsilon}\right)B=0 \quad \ldots\ldots\ldots\ldots\ldots (3)$$

To solve the above equation, we follow the prescription of Landau and Lifsitz and use $\boldsymbol{B}=u(z)\sqrt{\boldsymbol{\varepsilon}(z)}$, so that

$$\frac{d^2u}{dz^2}+k^2(\varepsilon-\sin^2\theta_i)u+\left(\frac{1}{2\varepsilon}\frac{d^2\varepsilon}{dz^2}-\frac{3}{4}\frac{1}{\varepsilon^2}\left(\frac{d\varepsilon}{dz}\right)^2\right)u=0 \quad \ldots\ldots\ldots (4)$$

In vacuum, $\varepsilon=1$, and $\dfrac{d\varepsilon}{dz}=0$, hence Equation (4) reduces to $\dfrac{d^2u}{dz^2}+k^2\cos^2\theta_i\,u=0$ and its solution is

$$\boldsymbol{u=A_0e^{-ik_zz}+B_0e^{ik_zz}} \quad \ldots\ldots\ldots\ldots\ldots\ldots\ldots\ldots\ldots\ldots (5)$$

with $k_z=\dfrac{\omega}{c}\cos\theta_i$.

In the bulk region, $\varepsilon=\varepsilon_b$, and $\dfrac{d\varepsilon}{dz}=0$, therefore Equation (4) reduces to

$\dfrac{d^2u}{dz^2}+k^2(\varepsilon_b-\sin^2\theta_i)u=0$, and its solution is given by

$$\boldsymbol{u=A_Ie^{-ik\sqrt{\varepsilon_b-\sin^2\theta_i}\cdot z}} \quad \ldots\ldots\ldots\ldots\ldots\ldots\ldots\ldots\ldots\ldots\ldots (6)$$

In the surface region,

$$\frac{d\varepsilon}{dz}=\frac{\varepsilon_b-1}{(z-d)}\frac{1}{\left[\log_e 2+(\varepsilon_b-1)\log_e(1-\frac{z}{d})\right]}$$

and $\dfrac{d^2\varepsilon}{dz^2}=\dfrac{-(\varepsilon_b-1)}{\log_e 2}\dfrac{1}{(z-d)^2}$.

As $\left[\dfrac{1}{2\varepsilon}\dfrac{d^2\varepsilon}{dz^2}-\dfrac{3}{4}\left(\dfrac{1}{\varepsilon}\dfrac{d\varepsilon}{dz}\right)^2\right]<<k^2(\varepsilon-\sin^2\theta_i)$, hence neglecting it, Equation (4) for the surface region become

$$\frac{d^2u}{dz^2} + (az+b)u = 0 \qquad \text{..... (7)}$$

Where, $a = \frac{k^2}{d\log_e 2}(1-\varepsilon_b)$ and $b = \frac{k^2}{2}$. The solution of Equation (7) can now be written as

$$u(z) = A_i(\xi) + B_i(\xi)$$

Where $\xi = \frac{-(az+b)}{a^{\frac{2}{3}}}$ and $A_i(\xi)$ and $B_i(\xi)$ are Airy functions (Ghatak *et al.,* 1995) given by,

$$A_i(\xi) = \left[3^{\frac{2}{3}}\Gamma\left(\frac{2}{3}\right)\right]^{-1}(1+\sqrt{3})\left(1+\frac{1}{3!}\xi^3+.....\right)$$

$$B_i(\xi) = \left[3^{\frac{1}{3}}\Gamma\left(\frac{1}{3}\right)\right]^{-1}(\sqrt{3}-1)\left(\xi+\frac{2}{4!}\xi^4+.....\right)$$

Absorbing the numerical coefficients and neglecting higher terms, we write the solution in the surface region as,

$$u(z) = A_2\left(1+\frac{1}{3!}\xi^3\right)+B_2\left(\xi+\frac{2}{4!}\xi^4\right) \qquad \text{..... (8)}$$

Using the boundary conditions that B and $\frac{\partial B}{\partial z}$ is continuous at $z=0$ and $z=-d$, we obtain for the three regions as

$$B(z) = \begin{cases} \left(e^{-ik\cos\theta_i\cdot z} + ye^{ik\cos\theta_i\cdot z}\right) & ;\ (vacuum) \\ p\left[\left(1+\frac{\xi^3}{6}\right)+x\left(\xi+\frac{\xi^2}{12}\right)\right](\varepsilon)^{\frac{1}{2}} & ;\ (surface) \\ pq\sqrt{\varepsilon_b}e^{-ik\sqrt{\varepsilon_b-\sin^2\theta_i}\cdot z} & ;\ (bulk) \end{cases} \qquad \text{..... (9)}$$

The electric field components can be obtained from the magnetic field by using the relation

$$E^x(\boldsymbol{K},\omega,z) = \frac{c}{i\omega\varepsilon}\frac{dB}{dz},$$

$$E^z(\boldsymbol{K},\omega,z) = -\frac{\sin\theta_i}{\varepsilon}B$$

Thus, we can write the vector potential in three regions as

$$\tilde{A}_\omega(z) = \frac{A^z_\omega(z)}{A_o} = \frac{E^z(\boldsymbol{K}\to 0,\omega,z)}{E_o} = \begin{cases} -\sin\theta_i\left[e^{-ik\cos\theta_i z} + ye^{ik\cos\theta_i z}\right], & (vacuum) \\ \frac{-\sin\theta_i}{\sqrt{\varepsilon}}p\left[1+\frac{\xi^3}{6}+x\left(\xi+\frac{\xi^4}{12}\right)\right], & (surface) \\ \frac{-\sin\theta_i}{\sqrt{\varepsilon_b}}pqe^{-ik\sqrt{\varepsilon_b-\sin^2\theta_i}\cdot z}, & (bulk) \end{cases} \qquad \text{.... (10)}$$

Various parameters in Equation (10) are defined as,

$$p = \frac{y+1}{\sigma + x\phi}, \quad q = \frac{1+\frac{\gamma^3}{6}+x\left(\gamma+\frac{\gamma^4}{12}\right)}{\sqrt{\varepsilon_b}e^{\lambda d}}, \quad x = \frac{a^{\frac{1}{3}}\sqrt{\varepsilon_b}\gamma^2+\left(\beta-\sqrt{\varepsilon_b}\lambda\right)\left[1+\frac{\gamma^3}{6}\right]}{\left(\sqrt{\varepsilon_b}\lambda-\beta\right)\left[\gamma+\frac{\gamma^4}{12}\right]-\sqrt{\varepsilon_b}a^{\frac{1}{3}}\left[1+\frac{\gamma^3}{3}\right]}$$

And $$y = \frac{ik\cos\theta_i(\sigma+x\phi)-\left[\frac{a^{\frac{1}{3}}}{2}\eta^2+\rho\sigma\right]+x\mu}{\frac{a^{\frac{1}{3}}}{2}\eta^2+\rho\sigma+x\mu+ik\cos\theta_i(\sigma+x\phi)} \quad \text{.....................................} (11)$$

Where, $\phi, \mu, \lambda, \beta$ etc. in Equation (11) are given by,

$$\sigma = 1+\frac{\eta^3}{6}, \quad \phi = \eta+\frac{\eta^4}{12}, \quad \mu = a^{\frac{1}{3}}\left(1+\frac{\eta^3}{3}\right)+\rho\phi, \quad \lambda = ik\sqrt{\varepsilon_b-\sin^2\theta_i}, \quad \beta = \frac{\varepsilon_b-1}{4d\sqrt{\varepsilon_b}\log_e 2},$$

$$\gamma = \frac{ad-b}{a^{\frac{2}{3}}}, \quad \eta = \frac{-b}{a^{\frac{2}{3}}} \text{ and } \rho = \frac{\varepsilon_b-1}{2d\log_e 2} \quad \text{..} (12)$$

Matrix Element

Matrix element in Equation (1) for transition from initial to final state can be written in expanded form for the three regions as

$$\langle\psi_f|H'|\psi_i\rangle = \int_{vac}\psi_f^* H'\psi_i d^3r + \int_{surf}\psi_f^* H'\psi_i d^3r + \int_{bulk}\psi_f^* H'\psi_i d^3r \quad \text{......} (13)$$

Where in each region, the wave functions and the vector potentials corresponding to that region have to be used. The final state wave function (ψ_f) is taken to be free electron type (Thapa and Kar, 1988) given by the following expression,

$$\psi_f(z) = \begin{cases} \left(\frac{m}{2\pi\hbar^2\mu}\right)^{\frac{1}{2}}\frac{2\mu}{\mu+k_f}e^{-\alpha|z|}e^{ik_f z}; & (z\le 0) \\ \left(\frac{m}{2\pi\hbar^2\mu}\right)^{\frac{1}{2}}\left[e^{i\mu z}+\frac{\mu-k_f}{\mu+k_f}e^{-i\mu z}\right]; & (z\ge 0) \end{cases} \quad \text{..................................} (14)$$

Where, $k_i^2 = \frac{2m}{\hbar^2}E_i$, $k_f^2 = \frac{2m}{\hbar^2}E_f$, $E_f = E_i + \hbar\omega$ and $\mu^2 = \frac{2m}{\hbar^2}\left(E_f - Vo\right)$.

Here, the factor $e^{-\alpha|z|}$ is introduced for the region $z \le 0$ to take into account the inelastic scattering of the electron (Pendry, 1976). To deduce the initial state wave function (ψ_i), Kronig Penney potential (Thapa and Kar, 1995) is used to define the crystal potential. In this, one generally solves the one dimensional Schrodinger's equation which can be written as

$$\frac{d^2\psi(z)}{dz^2}+k_i^2\psi(z) = -2V(z)\psi(z) \quad \text{...} (15)$$

Where $k_i^2 = \frac{2mE}{\hbar^2}$ and $V(z)$ is the δ-function potential of the Kronig-Penney model. Let $\phi(z)$ denote the Bloch wave function deep in the metal and $\phi^*(z)$ the time reversal version of $\phi(z)$. The eigenfunction in the semi-infinite solid ($z<0$) has been chosen to have the form

$$\psi_i(z) = \phi(z) - P\phi^*(z) \quad \text{...... (16)}$$

Where P is the reflection coefficient obtained by matching the wave functions and its derivative at $z=0$? One can then show that the initial state wave function for $z<0$ may be written as

$$\psi_i(z) = (1 - iPe^{-i\delta}\sin\delta)e^{ik_i(z)} - (P - ie^{i\delta}\sin\delta)e^{-ik_i(z)} \quad \text{...... (17)}$$

Where $\cot\delta = -\frac{\hbar^2 k_i}{mg}$ with g being the strength of the potential. The initial state wave function outside the metal ($z>0$) is

$$\psi_i(z) = Te^{-\chi z} \quad \text{...... (18)}$$

Where T is the transmission coefficient across the boundary plane and $\chi^2 = 2(V_o - E)$ with V_o being the step potential at the surface? By matching the wave function and its derivative at $z=0$, we get

$$P = \frac{(\chi - ik_i) - (k_i - i\chi)e^{i\delta}\sin\delta}{(\chi - ik_i) + (k_i - i\chi)e^{-i\delta}\sin\delta} \text{ and } T = \frac{2ik_i \sin 2\delta}{(\chi - ik_i) + (k_i - i\chi)e^{-i\delta}\sin\delta}.$$

Thus, the initial state wave function can be written as

$$\psi_i(z) = \begin{cases} \left(1 - iPe^{-i\delta}\sin\delta\right)e^{ik_i z} - \left(P - ie^{i\delta}\sin\delta\right)e^{-ik_i z} & (z \le 0) \\ Te^{-\chi z} & (z \ge 0) \end{cases} \quad \text{....(19)}$$

Using these expressions of ψ_f and ψ_i from Equations (14) and (19) and the vector potential as given by Equation (10), the matrix element in Equation (13) can be evaluated for each region to calculate photocurrent.

RESULTS AND DISCUSSION

The variation of vector potential as a function of photon energy for three locations of the surface plane has been calculated in the case of metals *W* and *Ni* and semiconductors *PbS* and *PbSe*. We have used the experimentally determined values of dielectric constants for calculating the vector potential in Equation (10). This value of vector potential had been used as a subroutine in the main FORTRAN programme to calculate photocurrent. We have used the following data for all the systems for calculating photocurrent. Here energy is measured from the bottom of the well.

Angle of incidence $\theta_i = 45^o$

Potential barrier height $V_o = 19.28$ eV

Initial state energy $E_i = 11.5$ eV.

(a) Tungsten: Figure 2 shows the plot of $|\tilde{A}_\omega(z)|^2$ against photon energy $(\hbar\omega)$ for locations of the surface plane at $z=-d$, $-\frac{d}{2}$ and 0 respectively. We find that for $z=-\frac{d}{2}$ (middle of surface width), as the photon energy is increased, the values of $|\tilde{A}_\omega(z)|^2$ increases and attains a maxima at $\hbar\omega = 21$ eV. As the value

of $\hbar\omega$ is further increased, $\left|\tilde{A}_\omega(z)\right|^2$ decreases and becomes minimum at $\hbar\omega = 28\,\text{eV}$. The plasmon energy of *W* is $\hbar\omega_p = 25.3\,\text{eV}$. It means that near about the plasmon energy of *W* $\left|\tilde{A}_\omega(z)\right|^2$ attains a minimum value. Beyond this value when $\hbar\omega$ increases a second hump in $\left|\tilde{A}_\omega(z)\right|^2$ is obtained at $\hbar\omega = 35\,\text{eV}$ and it decreases as $\hbar\omega$ increases. For $z = -d$ and $z = 0$, the plot does not show peaks neither before the plasmon energy nor after it rather we find a small hump at around 21 eV in both cases. The plot of photocurrent as a function of $\hbar\omega$ in the case of *W* with scattering factor $\alpha = 0.9$ and strength of the potential $g = 0.7$ is shown in Figure 3. We have shown the plots for two surface widths $d = 2.65$ Å (the curve with open circle) and narrow surface width $d = 0$ (the curve with closed circles). For $d = 2.65$ Å, we find that the photocurrent increases as $\hbar\omega$ increases and attains a maximum at $\hbar\omega = 19\,\text{eV}$. Further increase in photon energy ($\hbar\omega$) decreases the photocurrent and shows a minimum at $\hbar\omega = 25\,\text{eV}$. The plasmon energy of *W* is at $\hbar\omega = \hbar\omega_p = 25.3\,\text{eV}$. It means that the minimum in photocurrent occurs at plasmon energy.

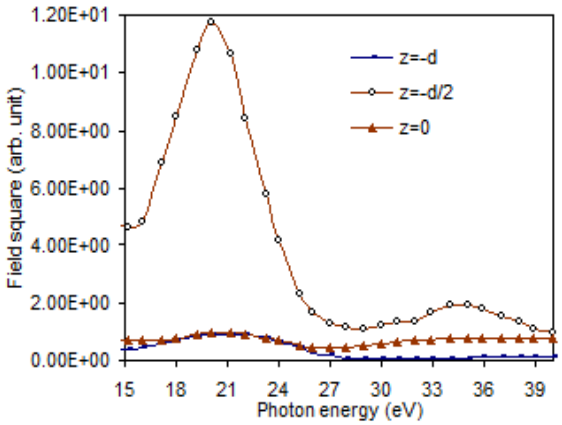

Figure 2: Plot of $\left|\tilde{A}_\omega(z)\right|^2$ as a function of $\hbar\omega$ for *W*

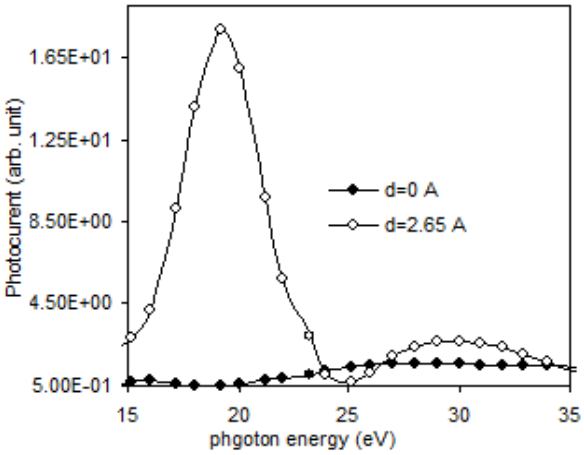

Figure 3: Plot of Photocurrent as a function of photon energy $\hbar\omega$ for *W*

This feature had been also seen in the experimental results (Weng *et al.,* 1978) and also in the calculated results of Bagchi and Kar (1978). We also did a calculation with a narrow surface width $d = 0$ (the curve with closed circle). We see that in this case, the minimum at the plasmon energy in the photocurrent plot is missing. This supports our conclusion that the inclusion of surface of certain width and spatial variation of vector potential is important in the analysis of photoemission data.

(b) Nickel: Figure 4 shows the variation of $\left|\tilde{A}_\omega(z)\right|^2$ as a function of photon energy for different values of the surface plane ($z = -d, z = -\frac{d}{2}, z = 0$). From the plot it is clear that the field for the middle of the surface $z = -\frac{d}{2}$ (the curve with open circle) shows a peak at around 11eV followed by a broad minimum from 18 to 24eV. Beyond 24eV, however the plot shows an increase in $\left|\tilde{A}_\omega(z)\right|^2$ as $\hbar\omega$ increases. Although the plot shows a broad minimum, the minimum is near the plasmon energy of *Ni* that is $\hbar\omega_p = 21eV$.

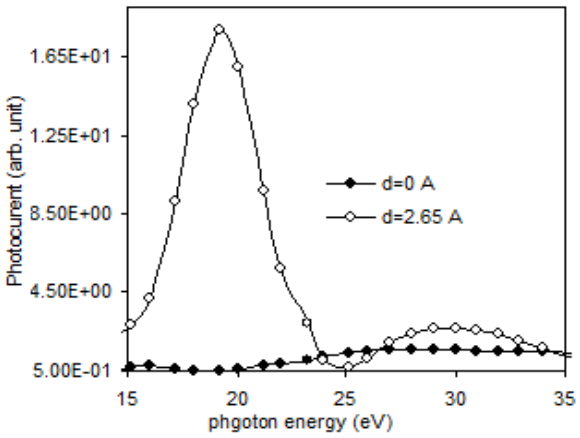

Figure 4: Plot of $|\tilde{A}_{\omega}(z)|^2$ as a function of $\hbar\omega$ for *Ni*

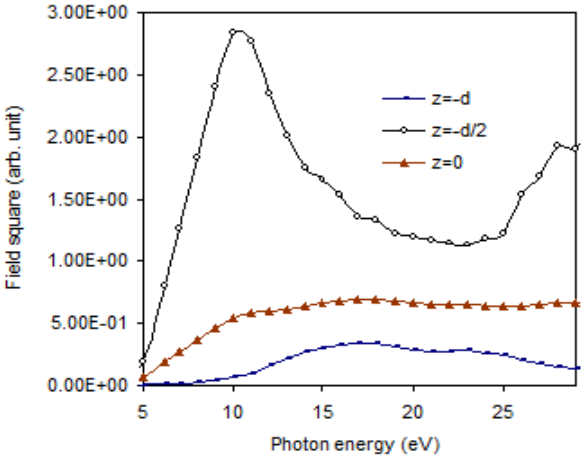

Figure 5: Plot of Photocurrent as a function of photon energy $\hbar\omega$ for *Ni*

In Figure 5, we have shown the results of the variation of photocurrent as a function of photon energy for surface width $d = 5.3$ Å and $d = 0$ (narrow surface) with scattering factor $\alpha = 0.9$ and strength of the potential $g = 0.7$. Just like in the case of metal *W*, the photocurrent plot for $d = 5.3$ Å (the curve with open circles) increases with the increase in photon energy and showed a maximum at $\hbar\omega = 18$ eV. A minimum in the photocurrent occurred at 23 eV with a second peak in photocurrent of a small height at $\hbar\omega = 25$ eV. The behavior in photocurrent showed trends similar to that in the case of *W*. For narrow surface width ($d = 0$), the photocurrent did not show any such features but instead remained constant for all values of photon energies.

(c) Lead Sulphide: Figure 6 shows the variation of $|\tilde{A}_{\omega}(z)|^2$ with photon energy for different values of surface plane ($z = -d, z = -\frac{d}{2}, z = 0$) in the case of *PbS*. For locations of the surface plane at $z = -\frac{d}{2}$, we find that the values of $|\tilde{A}_{\omega}(z)|^2$ showed a maxima at $\hbar\omega \approx 12$ eV, followed by a minimum at $\hbar\omega \approx 16$ eV. A second hump in $|\tilde{A}_{\omega}(z)|^2$ was found at $\hbar\omega = 18$ eV. As can be seen from the figure, the variation of $|\tilde{A}_{\omega}(z)|^2$ as a function of photon energy for other locations of the surface planes *i.e.* $z = -d$ and $z = 0$, is totally different from that in the case of $z = -\frac{d}{2}$ with no pronounced maximum and minimum.

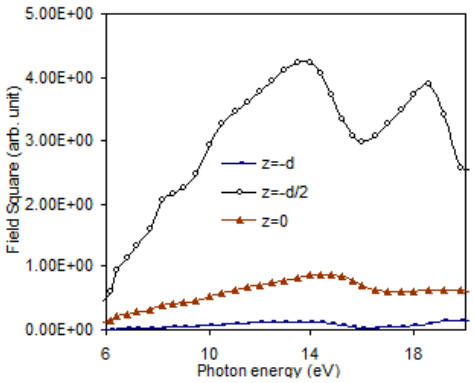

Figure 6: Plot of $|\tilde{A}_{\omega}(z)|^2$ as a function of $\hbar\omega$ for *PbS*

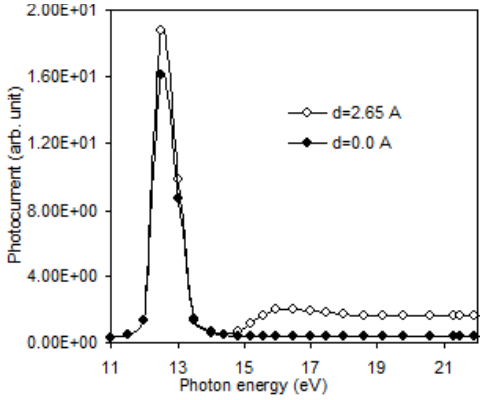

Figure 7: Plot of Photocurrent as a function of photon energy $\hbar\omega$ for *PbS*.

Figure 7 shows the plot of photocurrent against photon energy for *PbS* with scattering factor $\alpha = 0.5$, strength of the potential $g = 0.5$ and surface thickness $d = 2.65$ Å. The photocurrent plot for $d = 2.65$ Å (the curve with open circles) shows a peak around 13eV with a minimum at around 14.5eV followed by a second broad peak around 16eV. The photocurrent plot for a narrow surface width $d = 0$ (the curve with closed circles) shows a peak of lower height at around 13eV followed by a dip in photocurrent at 14.5eV, beyond which the photocurrent remains constant with further increase in photon energy. This shows that the surface effect is less prominent in case of semiconductor in contrast to the case of metals in which the surface effect is prominent.

(d) Lead Selenide: Figure 8 shows the plot of $\left|\tilde{A}_\omega(z)\right|^2$ against photon energy for different values of surface plane ($z = -d, z = -\frac{d}{2}, z = 0$). As can be seen from the figure, there is no pronounced peak or minimum even in the case of the plot for the middle of the surface plane *i.e.* $z = -\frac{d}{2}$ (the curve with open circles). It is seen that $\left|\tilde{A}_\omega(z)\right|^2$ initially increases with increase in photon energy ($\hbar\omega$), however instead of a peak and expected minimum at plasmon energy, it shows a plateau in the photon energy range 9 to 14eV. Beyond 14eV, there is a slight rise in $\left|\tilde{A}_\omega(z)\right|^2$ with further increase in photon energy. For $z = -d$, $\left|\tilde{A}_\omega(z)\right|^2$ practically remains constant for all values of photon energies while for $z = 0$, $\left|\tilde{A}_\omega(z)\right|^2$ shows a broad plateau extending from around 6eV to 14eV. However beyond 14eV, $\left|\tilde{A}_\omega(z)\right|^2$ shows a decrease with further increase in photon energy.

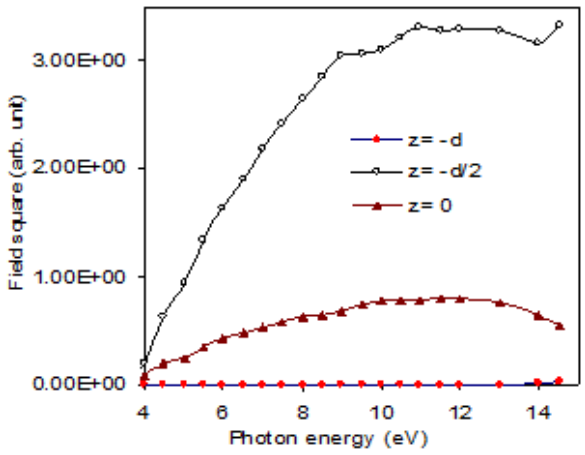

Figure 8: Plot of $\left|\tilde{A}_\omega(z)\right|^2$ as a function of $\hbar\omega$ for *PbSe*

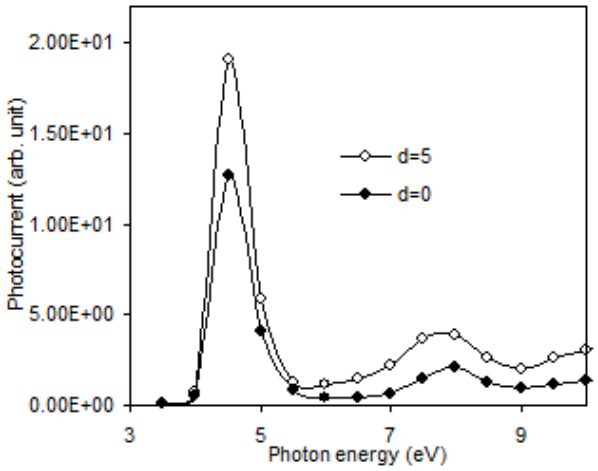

Figure 9: Plot of Photocurrent as a function of photon energy $\hbar\omega$ for *PbSe*

Figure 9 shows the variation of photocurrent in the case of *PbSe* as a function of photon energy with scattering factor $\alpha = 0.9$, the strength of the potential $g = 0.7$ and surface thickness $d = 5.3$ Å (the curve with open circles). The curve for $d = 5.3$ Å shows a minimum around 5.5eV. There is a maximum around 4.5eV and a broad maximum of much lower height at around 8eV. The plot of photocurrent for a narrow surface width $d = 0$ (the curve with closed circles) also shows similar trends apart from the

difference in the height of the peaks. This again supports our view that the surface characteristics are less pronounced in the semiconductors than in the case of metals.

CONCLUSION

The calculated result of photocurrent for the metals and semiconductors shows that our model gives results that agree qualitatively with the experimental results. We feel that a proper choice of crystal potential will enable us to obtain the initial state wave-function that is well-defined for the surface, bulk and the vacuum region unlike the K-P potential used here which gives the same initial state wave-functions for both the surface and bulk region. The initial state wave-function thus obtained will definitely give results that are much closer to the experimental results. From the results presented here, we can safely conclude that the dielectric model presented here does work well for metals especially in the case of *Al* (Gurung *et al.,* 2006) and *W*.

REFERENCES

Bagchi A and Kar N (1978). Refraction effects in angle-resolved photoemission from surface states on metals. *Physics Rev B* **18**(10) 5240-5247.

Das P, Thapa RK and Kar N (1991). Photoemission calculation with a simple model for the photon field: application to aluminium. *Modular Physics Letters B* **5**(1) 65-72.

Ghatak AK, Goyal IC and Chua SJ (1995). *Mathematical Physics* (Mc Millan India Limited) **66** 459.

Gurung S, Thapa RK, Das G and Bhattacharjee R (2006). Calculation of photocurrent in Al and Be by using the free electron potential model for the crystal. *Indian Journal of Physics* **80**(4) 361-366.

Landau LD and Lifsitz EM (1984). *The Electrodynamics of Continuous Media* (Pergamon Press, New York) **86** 293-304.

Pachuau Z, Gurung S, Thapa RK, Khating DT and Kar N (1999). Photocurrent calculations in semiconductors using Kronig-Penney model. *Indian Journal of Physics* **73A**(2) 237-243.

Pachuau Z, Zoliana B, Patra PK, Khating DT and Thapa RK (2002). Application of Mathieu potential to photoemission calculations: the case of a strong potential. *Physics Letters A* **294**(1) 52-57.

Pendry JB (1976). Theory of photoemission. *Surface Science* **57**(2) 679-705.

Penn DR (1972). Photoemission spectroscopy in presence of adsorbate-covered surfaces. *Physics Revision Letters* **28**(16) 1041-1044.

Thapa RK and Kar N (1988). Photoemission calculation from band states using Kronig-Penney model and spatially varying photon field. *Indian Journal of Pure and Applied Physics* **26**(10) 620-623.

Thapa RK (1993). Photoemission calculations using Kronig-Penney model and spatially dependent vector potential. *Physics Stat Sol (b)* **179**(2) 391-397.

Thapa RK, Das P and Kar N (1994). Photoemission calculation with Kronig-Penney model. *Modular Physics Letters B* **8** 361-366.

Thapa RK and Kar N (1995). Kronig-Penney model treatment of photoemission from silicon. *Surface Science* **338**(1-3) 138-142.

Weng SL, Gustaffson T and Plummer EW (1978). Experimental and theoretical study of the surface resonances on the (100) faces of W and Mo. *Physics Review B* **18**(4) 1718-1740.

Zaithanzauva and Thapa RK (1996). Photocurrent behaviour in free electron metals. *Indian Journal of Pure and Applied Physics* **34**(10) 843-844.